Astron. Astrophys. 349, 1003–1016 (1999)

ASTRONOMY AND ASTROPHYSICS

# An accretion-ejection instability in magnetized disks

**M. Tagger**[1] **and R. Pellat**[2]

[1] DSM/DAPNIA/Service d'Astrophysique (CNRS URA 2052), CEA Saclay, F-91191 Gif-sur-Yvette, France
[2] Centre de Physique Théorique, Ecole Polytechnique, Palaiseau, France

Received 12 January 1999 / Accepted 21 July 1999

**Abstract.** We present an instability occurring in the inner part of disks threaded by a moderately strong vertical (poloidal) magnetic field. Its mechanism is such that a spiral density wave in the disk, driven by magnetic stresses (rather than self-gravity as in galactic spirals), becomes unstable by exchanging angular momentum with a Rossby vortex it generates at its corotation radius. This angular momentum can then "leak" as Alfven waves emitted toward the corona of the disk thus providing, as an element of the accretion process, an energetic source for a wind or a jet. As galactic spirals, this instability forms low azimuthal wavenumber, standing spiral patterns which might provide an explanation for low-frequency QPOs in low-mass X-ray binaries.

**Key words:** accretion, accretion disks – instabilities – Magnetohydrodynamics (MHD) – waves – galaxies: jets

## 1. Introduction

The accretion disks of objects such as Active Galactic Nuclei, X-ray binaries or Young Stellar Objects are very commonly observed to emit jets, whose formation seems to be inherent to the accretion process. For instance in YSOs the power of the outflows has been found to be correlated with the accretion flux (Cabrit & André, 1991; Edwards et al., 1993). In the micro-quasar GRS 1915 recent multi-wavelength observations (Mirabel et al., 1998) show the ejection of plasmoids coinciding with the infall of the inner region of the disk toward the central black hole. It is thus considered as a strong point in favor of MHD models of jets that, from their very beginning, these models found that the jets are very efficient at carrying away the angular momentum extracted from the disk, and thus at permitting accretion to proceed. This has led to the success of a family of accretion-ejection models for these objects (see e.g. Blandford & Paine, 1982; Pelletier & Pudritz, 1992).

On the other hand existing models of turbulent accretion in disks always involve a transfer of angular momentum which is *radial*, *i.e.* within the disk: this is built into the ad-hoc model of $\alpha$ disks (Shakura & Sunyaev, 1973), where turbulence results in a viscous radial diffusion of the angular momentum. This is also true of specific models of disk instabilities (Papaloizou & Pringle, 1984; Tagger et al., 1990, hereafter paper I; Balbus & Hawley, 1991) which all rely, in one form or another, on a radial exchange of angular momentum. This may appear as a contradiction between disk and jet models. We believe that it is one of the main reasons why it has always been very difficult, though not totally impossible, to develop models connecting jet solutions to disk models (Ferreira & Pelletier, 1993; Ogilvie & Livio, 1998), in such a manner that the angular momentum of accretion is redirected toward the jet.

We present in this paper a new instability mechanism which might help solve this contradiction. The instability appears in the innermost region of the disk (a few times the inner radius), where roughly half of the accretion energy and angular momentum must be disposed of. Its physics is such that the angular momentum extracted from the disk is not emitted radially but will ultimately end up as an Alfven wave traveling to the disk corona, where it can thus power the jet.

This results from the combination of three ingredients:

- We have shown in previous work (Paper I) that spiral waves driven by magnetic stresses (rather than by self-gravity as in galactic disks) propagate in disks threaded by a vertical (poloidal) magnetic field. One can thus consider that the family of spiral density waves in disks concerns disks with an attractive long-range force (self-gravity) as in spiral galaxies, disks with only the local pressure force (giving the Papaloizou-Pringle instability), and disks with a repulsive long-range force, resulting from magnetic stresses. These waves can be amplified in the region of their corotation radius. The amplification is strong for self-gravity driven waves, and very weak in the other cases. However the Papaloizou-Pringle instability concerns only waves with very small wavelengths (of the order of the disk thickness), whereas self-gravity or magnetic stresses move the unstable range to larger scales (small azimuthal wavenumber).
- Our result, as well as most of the theoretical work on the propagation and amplification of spirals, was obtained in the classical shearing sheet model, which allows a thorough analysis of the physical processes involved but neglects an important effect: the gradient of vorticity in the equilibrium

*Send offprint requests to*: M. Tagger (tagger@cea.fr)

flow of the disk, and as a consequence the *corotation resonance*, whereby the density waves couple to a vortex at their corotation radius[1]; in a paper to be published independently we will present an extension of the shearing sheet model, keeping into account the vorticity gradient in the disk, and thus the physics of the corotation resonance. It will allow us to analyze in more details the coupling to this vortex, which is in fact a Rossby wave, associated with the vorticity gradient in the disk; the propagation of the Rossby wave is quenched by differential rotation, but this still allows it to exchange energy and momentum with the density wave. In the present paper we will only use the exact cylindrical geometry, so that the physics of Rossby waves is fully taken into account.

The effect of this resonance is only minor for self-gravity driven spirals, which are very unstable anyway (Pannatoni, 1983). It does not change much the order of magnitude of the growth rate for the Papaloizou-Pringle instability (Papaloizou & Pringle, 1985; Narayan et al., 1987). It has not been considered thus far for the magnetically driven spirals.

– On the other hand, we should expect a strong influence in the magnetically driven case: in the Papaloizou-Pringle instability, density waves are evanescent in the corotation region and are thus exponentially small at the corotation radius, where they couple to the vortex. In the magnetically driven case, density waves create magnetic perturbations which decrease only weakly in the corotation region. This allows their coupling to the vortex to be much more efficient. More precisely we will find the coupling algebraically, rather than exponentially, small, the small parameter being essentially $m$ (the azimuthal wavenumber) times the ratio of the disk thickness to radius. We will find this sufficient to get a sizable amplification of the density wave.

We will show that this instability forms *normal modes*, *i.e.* standing, exponentially growing patterns. They are localized close to the inner radius of the disk, and thus cannot be considered to cause accretion in a large portion of it. However in this inner region, where roughly half of the accretion energy and angular momentum are generated, they can cause accretion and energize a jet.

One can have two views of this amplification process: we can consider it, as we did above, as the amplification of the spiral wave by interaction with the Rossby vortex it generates. But we can also concentrate on the evolution of the vortex: differential rotation leads it to be sheared away as time evolves, so that an initially leading pattern becomes strongly trailing; but at the same time the vortex generates a spiral density wave which, after reflection at the inner radius of the disk, returns to regenerate it as a leading feature, starting a new cycle.

We present two complementary computations of the amplification due to this resonance. The first approach is analytical, in the form of a variational principle which allows us to discuss the physics, the sign and the order of magnitude of the amplification. We find in particular that the parameter controlling the sign of the resonant effect is not as usual the gradient of the specific vorticity in the equilibrium flow, but a different quantity involving the magnetic field strength. This first approach allows us to extract and describe in details the physical processes involved in the formation of normal modes and in their amplification.

In a second step we present numerical solutions which confirm this behavior, and allow us to exhibit exponentially growing normal modes affecting the inner region of the disk. Their growth time is typically a fraction of the rotation time of the disk at the corotation radius.

We derive both of these results in the simple model of an infinitely thin disk in vacuum. In this case the energy and angular momentum extracted from the inner region have to stay in the disk: they are stored in the vortex at corotation, rather than carried away by a density wave travelling outward as in the usual amplification process of spiral density waves. In the Papaloizou-Pringle case, Narayan et al. (1987) have argued that the accumulation of angular momentum in the vortex might eventually saturate at a finite amplitude, thus ending the amplification process. We will briefly discuss how here, if the disk were more realistically embedded in a low density corona, the angular momentum would be emitted as an Alfven wave emitted vertically along the field lines. We will reserve the detailed discussion and computation of this effect to a forthcoming publication. In our conclusion we will discuss possible astrophysical consequences of this new mechanism.

Throughout this paper we will consider *normal modes*, *i.e.* exponentially growing perturbations characterized by a single frequency $\omega$. As usual in disks with differential rotation, the amplification mechanism would also apply to transient shearing perturbations, which become normal modes only when a reflexion at the inner radius allows them (if they obey an integral phase condition) to start a cycle of wave reflection and amplification. The amplification process is the same. However it is weak enough that the transient amplification of perturbations starting at the noise level is probably insufficient to cause accretion; thus only normal modes, whose exponential growth allows them to reach large amplitudes, should really matter in accretion disks.

Curry & Pudritz (1996) have performed a modal analysis of an MHD disk, in an incompressible MHD cylinder limit. Incompressibility did not allow them to make a connection with the magnetized spirals of paper I, and thus to identify the effects discussed here. They study in details the Alfven resonance ($\omega - m\Omega(r) = k_z v_A$, where $k_z$ is a vertical wavenumber), which is very close to corotation where our main effect occurs (corotation is not a singularity in their approximation). It is very likely that the Alfven resonance is a form of the coupling to vertically propagating Alfven waves which will be briefly discussed below. However in the context of our modes, which are essentially constant over a disk scale height, $k_z$ looses its meaning and this would need to be studied with a more elaborate treatment of the vertical dimension, giving the vertical ejection of angular momentum associated with our modes. We defer this to a future

[1] the radius where the angular phase velocity of the wave equals the angular velocity of the gas, not to be confused with the radius where the gas rotates at the angular velocity of the central object.

publication, and will present in Appendix C only a brief sketch of the coupling with Alfven waves far from this resonance.

## 2. The basic model

### *2.1. Thin disk geometry and relation with other instabilities*

We restrict ourselves to perturbations of an infinitely thin disk, neglecting vertical velocities and variations of the perturbations across the disk. This means that we will not discuss the magneto-rotational instability (Velikhov, 1959; Chandrasekhar, 1960; Balbus & Hawley, 1991), which relies on the existence of a wavelength in the vertical direction. In a previous work (Tagger et al., 1992) we discussed the vertical structure of disk perturbations, and showed that there always exists a solution with weak variations across the disk; this solution reduces, to lowest order in the disk aspect ratio (thickness/radius), to the infinitely thin solution considered here.

Thus we will totally discard here the vertical structure of the wave within the disk, which is essential to the magneto-rotational instability. There are two reasons for this: one is that these instabilities are entirely distinct and proceed from very different mechanisms; the second reason is that the magneto-rotational instability occurs only when the magnetic pressure is weak, *i.e.* the ratio $\beta = 8\pi p/B^2$ of the thermal to magnetic energy density is larger than one whereas, as will be seen below, our instability is significant only when $\beta$ becomes of the order of one, or weaker. We will thus consider disks where the magnetic pressure is strong, in the sense that $\beta \lesssim 1$, but still much weaker than the gravitational energy so that magnetic support of the disk remains weak. When magnetic support becomes strong our instability becomes the interchange mode studied by Spruit and coworkers (Spruit & Taam, 1990; Spruit et al., 1995) in disks with and without differential rotation. Indeed our basic assumptions are essentially the same as theirs. In an approximate analysis of the effect of differential rotation Spruit et al. (1995) found that it makes the amplification of the interchange mode only transient, and negligible unless the magnetic field is very strong. In fact the vortex part of our instability may be viewed in some respects as an interchange, since the vortex effectively exchanges flux tubes across the corotation radius, and the amplification relies on the radial gradients of $B_0$ and $\Sigma$ (the surface density) – although in a different form than that found by Spruit et al.. The coupling between the vortex and density waves, which allows the formation of exponentially growing normal modes, allows our instability to act already at $\beta \sim 1$, *i.e.* at much lower magnetic pressure than in their case. A more detailed comparison is difficult, because we use a slightly different model: Spruit et al. consider magnetic fields supported by equilibrium currents only in the disk, resulting in a jump of $B_r$ across the disk, whereas for simplicity we assume that the magnetic field gradient at equilibrium is only due to external currents (e.g. ring currents inside the inner disk radius), so that the equilibrium field is purely vertical across the disk.

Our justification for this is that we are interested in a regime where the interchange instability should be negligible. On the other hand in more recent work, Stehle & Spruit (1998) found in non-linear simulations strong instabilities even in situations which should be stable to the interchange mode. It is possible that this is a manifestation of the instability we present here (in particular the density and magnetic field profiles they use should give instability, according to our criterion). But the growth rates they find are rather large, and the modes have a more global structure than we would expect. Although no definite conclusion can be reached at this stage, we rather believe that their result is due to the reflective boundary condition they use at large $r$: in the Papaloizou-Pringle case (Narayan et al., 1987) and presumably also in the magnetic case, this leads to a strong form of the spiral instability, due to the formation of a double cavity between the corotation radius and the inner and outer radii of the disk. This boundary condition, often used in disk theories and simulations, can thus be quite misleading, although one might look for astrophysical justifications in specific contexts, if some mechanism can act to truncate the disk at large radii. Otherwise a radiation condition at the outer radius must be used, as we do here. Simulations with different boundary conditions, or increased outer radius, would then be necessary to fully understand their result.

Our simple model of a disk in vacuum also means that we cannot fully justify, in the limits of the present paper, our claim that our instability may eventually redirect toward the disk corona the angular momentum it extracts from the disk. This can however be easily understood if one remembers that the disk is threaded by magnetic field lines, along which Alfven waves can propagate as soon as there is any small plasma density in the corona of the disk; the vortex at the corotation radius moves the footpoints of the magnetic field lines, and this motion (of torsional nature, whereas the motion associated with the spiral is essentially compressional) will act as an initial condition for the emission of Alfven waves. We can thus consider that, although this is not contained in the present description where the disk is in vacuum, the energy and angular momentum deposited in the vortex by the instability will end up in these Alfven waves propagating in the corona. In Appendix C we show how this occurs in the region where density waves propagate, in the WKB approximation. The full computation, valid in the corotation region, is much more complex and we defer it to a future publication.

### *2.2. The magnetic field*

We consider a disk threaded by a vertical magnetic field. For simplicity we discard radial or azimuthal (toroidal) components of the equilibrium magnetic field, and assign its radial dependence to external currents[2]. Thus at equilibrium the disk is characterized by its surface density $\Sigma(r)$ and magnetic field $\boldsymbol{B} = B_0(r)\boldsymbol{e}_z$.

[2] This choice is made in order to trim down our model to the minimal necessary physics, for the sake of clarity in this paper where we wish to present and discuss the basic physics of our instability. Taking into account equilibrium currents in the disk, which cause a finite inclination of the field lines at its surface, is straightforward, and preliminary results show that they increase significantly the growth rate of the instability.

The disk lies in vacuum: then the absence of currents allows us to describe the perturbed magnetic field outside the disk by a magnetic potential:

$$\boldsymbol{B} = -\mathrm{sign}(z)\boldsymbol{\nabla}\Phi_M \tag{1}$$

with

$$\Delta\Phi_M = 0. \tag{2}$$

We work in cylindrical coordinates $(r,\ \vartheta,\ z)$. The sign of $z$ in Eq. (1) ensures that, if $\Phi_M$ is even in $z$, the perturbed vertical field is also even, while its horizontal ($r$ and $\vartheta$) components are odd. From their change across the disk we get the currents:

$$\begin{aligned} j_r &= 2\frac{\partial}{\partial\vartheta}\Phi_M\delta(z) \\ j_\vartheta &= -2\frac{\partial}{\partial r}\Phi_M\delta(z) \end{aligned}$$

and the horizontal magnetic stresses acting on the disk:

$$\begin{aligned} F_M^r &= -2B_0\frac{\partial}{\partial r}\Phi_M\delta(z) \\ F_M^\vartheta &= -2B_0\frac{\partial}{\partial\vartheta}\Phi_M\delta(z) \end{aligned}$$

On the other hand the vertical component of the field:

$$B_z = -\mathrm{sign}(z)\frac{\partial}{\partial z}\Phi_M$$

gives at the disk:

$$\frac{\partial^2}{\partial z^2}\Phi_M = -2B_z^D\delta(z)$$

where $B_z^D$ is the perturbed field in the disk. Thus throughout space we can write:

$$\Delta\Phi_M = -2B_z^D\delta(z) \tag{3}$$

This can be compared with the Poisson equation giving the perturbed gravitational potential in a self-gravitating disk:

$$\Delta\Phi = 4\pi G\sigma\delta(z) \tag{4}$$

where $\sigma$ is the perturbed surface density. We can thus compute the magnetic potential by the classical Poisson Kernel (Binney & Tremaine, 1987): assuming perturbations varying as $\exp(im\vartheta)$ we have:

$$\Phi_M(r) = \int dr' K_m(\frac{r'}{r})B_z^D(r') \tag{5}$$

where

$$K_m(x) = \frac{x}{\pi}\int_0^\pi \frac{d\vartheta\cos m\vartheta}{(x^2-2x\cos\vartheta+1)^{1/2}} \tag{6}$$

### 2.3. Perturbation equations

We write the linearized Euler equations for perturbations varying as $e^{i(m\vartheta-\omega t)}$:

$$\begin{aligned} -i\tilde{\omega}v_r - 2\Omega v_\vartheta &= \frac{F_r}{\Sigma} \\ -i\tilde{\omega}v_\vartheta + Wv_r &= \frac{F_\vartheta}{\Sigma} \end{aligned}$$

where the forces in the right-hand sides comprise pressure and magnetic stresses. Here $\tilde{\omega} = \omega - m\Omega(r)$, $\Omega$ is the rotation frequency of the equilibrium flow, and $W$ is known in the context of galactic disks as Oort's second constant[3]:

$$W = \frac{\kappa^2}{2\Omega} = \frac{1}{r}\frac{d}{dr}(r^2\Omega)$$

$\kappa$ is the epicyclic frequency, and it is worth noting already at this point that $W$ is the vertical component of the vorticity of the equilibrium flow.

We find it more simple to change variables to:

$$\begin{aligned} s &= \ln r \\ U &= rv_r \\ V &= rv_\vartheta \end{aligned}$$

We get:

$$-i\tilde{\omega}U - 2\Omega V = -c_S^2\frac{\partial}{\partial sh} - 2\frac{B_0}{\Sigma}\frac{\partial}{\partial s\Phi_M} \tag{7}$$

$$-i\tilde{\omega}V + WU = -imc_S^2h - 2im\frac{B_0}{\Sigma}\Phi_M \tag{8}$$

where we have defined

$$h = \frac{\sigma}{\Sigma},$$

$\sigma$ is the perturbed density, and $c_S$ is the sound speed. For simplicity we have assumed an isothermal equation of state, and we will consider throughout this paper that $c_S$ is constant. We also write the continuity equation:

$$-i\tilde{\omega}r^2\sigma = -\frac{\partial}{\partial s}(\Sigma U) - im\Sigma V \tag{9}$$

Our system of equations is closed by the vertical component of the induction equation:

$$-i\tilde{\omega}r^2B_z^D = -\frac{\partial}{\partial s}(B_0U) - imB_0V \tag{10}$$

which can be usefully compared with Eq. (9): they correspond respectively to the conservation of magnetic flux and total density in a flux tube. Let us now consider Eqs. (9-10) and (4-3). The parallel between $\sigma$ and $B_z$, $\Phi$ and $\Phi_M$, shows that, as explained in paper I, the magnetic field appears in the mathematical form of a negative self-gravity, *i.e.* a long-range force whose action is repulsive (the magnetic field stiffening the field lines and thus resisting, rather than favoring, the formation of overdensities). We will hereafter, for simplicity, assume that the self-gravity of the disk is negligible but its inclusion in our description to discuss more massive disks would be straightforward.

[3] we will not use here the more classical notation $B$, in order to avoid confusion with the magnetic field

## 3. Corotation and amplification

### *3.1. A variational principle*

In this section we derive a variational principle which will allow us to analyze the effect of the corotation resonance, and also to discuss the boundary conditions to be used. As usual with variational formulations, this permits a more rigorous and general result than in previous discussions of both the resonance and the boundary conditions. In order to minimize the complexity, we present here only a simplified form retaining only magnetic stresses; the full computation, including pressure forces, is given in Appendix A.

We start from Eqs. (7–8), which give:

$$U = \frac{1}{L}\left\{-2i\tilde{\omega}\frac{B_0}{\Sigma}\frac{\partial}{\partial s}\Phi_M + 4im\Omega\frac{B_0}{\Sigma}\Phi_M\right\} \tag{11}$$

$$V = \frac{1}{L}\left\{-2W\frac{B_0}{\Sigma}\frac{\partial}{\partial s}\Phi_M + 2m\tilde{\omega}\frac{B_0}{\Sigma}\Phi_M\right\} \tag{12}$$

where

$$L = \tilde{\omega}^2 - \kappa^2$$

Substituting into Eq. (10), and using:

$$W = 2\Omega + \Omega', \quad \frac{\partial}{\partial s}\tilde{\omega} = -m\Omega'$$

where the prime denotes the derivative with respect to $s$, we get:

$$\begin{aligned} i\tilde{\omega}r^2\ B_z^D = &-i\tilde{\omega}\frac{\partial}{\partial s}\left\{2\frac{B_0^2}{\Sigma L}\frac{\partial}{\partial s}\Phi_M\right\} \\ &+\Phi_M\left[\frac{\partial}{\partial s}\left(\frac{4im\Omega B_0^2}{\Sigma L}\right) + 2im^2\frac{B_0^2}{\Sigma}\frac{\tilde{\omega}}{L}\right] \end{aligned} \tag{13}$$

After some algebra we write this as:

$$\begin{aligned} r^2 B_z^D = &-\frac{\partial}{\partial s}\left(\frac{2}{L}\frac{B_0^2}{\Sigma}\frac{\partial}{\partial s}\Phi_M\right) \\ &+\frac{2B_0^2}{\Sigma L^2}\Phi_M\left\{m^2\left(L + 4\Omega\Omega'\right)\right. \\ &\left.+2m\Omega\left[\tilde{\omega}\frac{\partial}{\partial s}\left(\ln\frac{\Omega B_0^2}{\Sigma}\right) + 2\frac{\Omega W}{\tilde{\omega}}\frac{\partial}{\partial s}\left(\ln\frac{W\Sigma}{B_0^2}\right)\right]\right\} \end{aligned} \tag{14}$$

We multiply both sides of this equation by $\Phi_M^*$ (where the star indicates the complex conjugate) and integrate over $s$ between boundaries $s_{min}$ and $s_{max}$. After an integration by parts we get a quadratic form:

$$\begin{aligned} \int_{s_{min}}^{s_{max}} ds\ &\left\{r^2(s)\Phi_M^*(s)B_z^D(s)\right. \\ &-\frac{2}{L}\frac{B_0^2}{\Sigma}\left|\frac{\partial}{\partial s}\Phi_M\right|^2 \\ &-\frac{2B_0^2}{\Sigma L^2}\left|\Phi_M\right|^2\left\{m^2\left(L + 4\Omega\Omega'\right)\right. \\ &\left.\left.+2m\Omega\left[\tilde{\omega}\frac{\partial}{\partial s}\left(\ln\frac{\Omega B_0^2}{\Sigma}\right) + 2\frac{\Omega W}{\tilde{\omega}}\frac{\partial}{\partial s}\left(\ln\frac{W\Sigma}{B_0^2}\right)\right]\right\}\right\} \\ = &-\left[\frac{2}{L}\frac{B_0^2}{\Sigma}\Phi_M^*\frac{\partial}{\partial s}\Phi_M\right]_{s_{min}}^{s_{max}} \end{aligned} \tag{15}$$

Let us consider the first term in the integral, in the left-hand side of this equation: using (5) we can write it as:

$$\int ds\, r^2 B_z^D(s) \int ds'\, r' K_m\left(\frac{r'}{r}\right) B_z^{D*}(s')$$

Using the property that:

$$K_m\left(\frac{1}{x}\right) = \frac{1}{x}K_m(x)$$

we see that this expression is hermitian (symmetric to the exchange of $B_z^D$ and $B_z^{D*}$).

Let us now consider the other terms in the left-hand side of Eq. (15): they have resonant denominators at $L = 0$ (the Lindblad resonances, $\tilde{\omega} = \pm\kappa$) and at $\tilde{\omega} = 0$ (the corotation radius). We will admit without demonstration the common result (obtained by a Frobenius expansion) that the solutions are regular at Lindblad resonances (Narayan et al., 1987), but not at corotation where the waves can exchange energy with the flow. This resonance has been discussed by Pannatoni (1983) in the context of galactic spiral waves, and by Papaloizou & Pringle (1985) and Narayan et al. (1987) in the context of the Papaloizou-Pringle instability. Its effect on the magnetically driven spiral density waves is the main object of this paper.

The corotation resonance appears only in the last term in the integral, on the left-hand side of Eq. (15). As will be seen later, it contributes an imaginary term to the integral and thus makes it non-hermitian. We will consider, as in the above-mentioned treatments, that this term is small (this can be obtained by reducing the derivative of $B_0^2/W\Sigma$), so that we can treat it as a perturbation. Then to lowest order, all the terms in the left-hand side are Hermitian, and the right-hand side is a boundary term (containing the physics associated with boundary conditions, as will be discussed below). This means that Eq. (15) is self-adjoint, so that it forms a variational principle (Morse and Feschbach, 1953). Appendix A shows that, as could be expected, this property is still valid when we retain pressure forces.

For readers not familiar with variational principles, we will only mention here their main advantage, namely that they allow a rigorous treatment of perturbation problems: let us note the variational form as:

$$\langle\xi^*|\mathcal{L}(\omega)|\xi\rangle = 0$$

where $\mathcal{L} = \mathcal{L}_0 + \varepsilon\mathcal{L}_1$, $\varepsilon$ is a small parameter and $\xi$ is the vector formed from the components (velocities, potential, density) of the perturbation. We assume that we know ($\omega_0,\ \xi_0$), an eigenvalue and eigenvector (the frequency and spatial dependence of the solution) of the unperturbed problem $\mathcal{L}_0$:

$$\mathcal{L}_0(\omega_0)\xi_0 = 0$$

and look for solutions ($\omega_0 + \delta\omega,\ \xi_0 + \delta\xi$) of the perturbed problem, to first-order in $\varepsilon$. The hermiticity of $\mathcal{L}_0$ gives

$$\langle\xi_0^*|\mathcal{L}_0(\omega_0)|\delta\xi\rangle = \langle\delta\xi^*|\mathcal{L}_0(\omega_0)|\xi_0\rangle = 0$$

so that $\delta\omega$ can be obtained to first order without need to compute $\delta\xi$, making the task relatively simple and more straightforward than the "direct" approach used e.g. by NGG. One gets simply:

$$\left\langle \xi_0^* \left| \frac{\partial \mathcal{L}_0}{\partial \omega} \right| \xi_0 \right\rangle \delta\omega = -\varepsilon < \xi_0^* | \mathcal{L}_1(\omega_0) | \xi_0 > \qquad (16)$$

In Sect. 3.2 we discuss the main properties of the unperturbed solutions. Since this neglects the corotation resonance, they are essentially the properties of magnetically-driven spiral waves, which had been obtained in the shearing-sheet approximation in Paper I. In Sect. 3.3 we will perturb them by the corotation resonance term. The boundary conditions, appearing in the right-hand side of Eq. (15), are discussed separately in Appendix B and implemented in the numerical solution presented in Sect. (4).

### *3.2. Waves and modes*

In this sub-section we discuss waves and modes, as they can be obtained from a WKB approximation in the unperturbed state (without the corotation resonance). The WKB approximation applies for spiral waves when the radial wavenumber is much larger than the azimuthal one (giving tightly wound spirals). Then the first two terms, on the left-hand side of Eq. (15) are larger than the other ones, which are proportional to $m$. We look for a local radial wavenumber $k$:

$$\frac{\partial}{\partial s}\Phi_M \approx ik(s)\Phi_M$$

and use the relation between $\Phi_M$ and $B_z^D$:

$$B_z^D = -\left[\frac{\partial}{\partial z}\Phi_M\right]_{z=0^+}$$

together with Eq. (2) which gives:

$$\frac{\partial}{\partial z}\Phi_M = -\frac{|k|}{r}\Phi_M$$

where the minus sign comes from the constraint that $\Phi_M$ decreases at $z \to \infty$. Then from the first two terms in Eq. (15) we get the dispersion relation:

$$\tilde{\omega}^2 = \kappa^2 + \frac{2B_0^2}{\Sigma}\frac{|k|}{r} + \frac{k^2}{r^2}c_S^2 \qquad (17)$$

where for completeness we have added the pressure term, derived from the full variational principle in Appendix A. This is the dispersion relation derived in paper I in the shearing sheet approximation. It is identical to the dispersion relation of self-gravity driven spiral density waves, with the magnetic term acting as a negative self-gravity.

From this dispersion relation one gets the basic properties of these waves: one can have both *leading* ($k < 0$) and *trailing* ($k > 0$) waves, resulting in spiral structures wound in opposite directions. Their group velocities, on both sides of corotation, are respectively toward and away from the corotation radius (where $\tilde{\omega}$ vanishes).

The waves propagate only where Eq. (17) has a positive root for $|k|$, *i.e.* for $\tilde{\omega}^2 - \kappa^2 > 0$ (beyond the Lindblad resonances). In the corotation region they are evanescent. Thus a leading wave traveling from the center toward corotation will be reflected at the Inner Lindblad Resonance (ILR) as a trailing wave traveling back toward the center. If the boundary condition at or near the center is, as usually considered, such that this trailing wave is reflected again as a leading wave, one can establish a cavity between the center and the ILR; for a discrete set of frequencies, given by an integral phase condition, the resulting leading wave has the same phase as the initial one, so that a standing pattern can be established. These patterns are known as normal modes of the system.

Another property of the waves is that they have a *negative energy* inside corotation, because they rotate slower than the gas, and positive energy outside. If the waves can tunnel through the forbidden band at corotation, they are amplified: let us explain this by considering a leading wave of energy -1 traveling from the center to the ILR, resulting by tunnel effect in the emission beyond the Outer Lindblad Resonance (OLR) of a trailing wave of energy $+\varepsilon$, unspecified but positive. Then the trailing wave reflected to the center must have energy $-1-\varepsilon$, *i.e.* a higher amplitude than the incoming wave: as it is reflected at the ILR, the wave is amplified.

In the case of the Papaloizou-Pringle instability, where the only force comes from the pressure (which acts only locally), $\varepsilon$ is exponentially small: this is natural since the waves are evanescent in the forbidden band, as usual with tunnel effects, so that the energy of the transmitted wave is proportional to the exponential of a large negative quantity, of the order of $-r\Omega/c_S$. However we have shown in PTS and paper I that the long-range nature of the forces change this result in the case of self-gravity driven or magnetically driven spirals. This appears mathematically, in the shearing sheet model, as the contribution of a branch cut in the complex-$k$ space, related to the spatial behavior of the potentials. The reason is in fact quite simple: consider a density perturbation in the cavity between the center and the ILR. The tunnel effect allows it to act beyond the forbidden band, in the same manner as in the Papaloizou-Pringle case. However, this density perturbation creates a potential which is *not* evanescent in the forbidden band! As usual for an $m$-polar potential, it varies as $r^{-m}$, so that it decreases only algebraically across the corotation region. This radial dependence corresponds to the fact that the branch cut found in $k$-space starts from singular points at $k = im$, or $k_x = ik_y$ in the cartesian geometry of the shearing sheet.

The result of this anomalous tunneling is that, for self-gravity driven spirals, $\varepsilon$ can be very large, rather than exponentially small as in the Papaloizou-Pringle case. In the magnetically driven case, we found in Paper I that maximal amplification is shifted to smaller azimuthal wavenumber, but remains small. We show in the next sub-section that the corotation resonance can make it much larger.

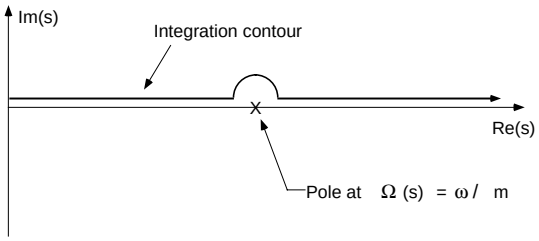


**Fig. 1.** The integration path for the integral in Eq. (18). The contour lies on the real axis (giving a real Principal Part), except for a clockwise semi-circle around the corotation pole.

### *3.3. Resonant effect at corotation*

We can now turn to the perturbative treatment of the corotation resonance. For simplicity we will neglect boundary terms (the right-hand side of Eq. (15)), treated separately in Appendix B. We thus rewrite Eq. (15) as:

$$\int_{s_{min}}^{s_{max}} ds \left\{ r^2(s)\Phi_M^*(s)B_z^D(s) - \frac{2}{L}\frac{B_0^2}{\Sigma}\left|\frac{\partial}{\partial s}\Phi_M\right|^2 - \frac{2B_0^2}{\Sigma L^2}\left|\Phi_M\right|^2 \mathcal{O}(m)\right\} = \int_{s_{min}}^{s_{max}} ds \quad \frac{8m\Omega^2 W}{\tilde{\omega}}\frac{B_0^2}{\Sigma L^2} \quad \left|\Phi_M\right|^2 \frac{\partial}{\partial s}\left(\ln\frac{W\Sigma}{B_0^2}\right) \qquad (18)$$

where $\mathcal{O}(m)$ contains terms we neglected in the WKB approximation; we will also neglect them here as in the "cavity" where the waves propagate (so that $\Phi_M$ is large) these terms are small. To lowest order (*i.e.* neglecting the right-hand side) this equation gives a discrete spectrum of normal modes, discussed in the previous sub-section, which are neither amplified nor damped (since the operator is hermitian, $\omega$ is real).

To the next order we perturb these solutions by the resonant term in the right-hand side, using Eq. (16). We are only interested in the imaginary part of the integral in the right-hand side, since it will give us the growth rate resulting from the resonance. This is done in the classical way used to study Landau damping in plasmas, or similar fluid problems (Lin, 1955, Narayan et al., 1987), and for completeness we will sketch here its justification. One must remember that, since the modes we are looking for are exponentially growing or decreasing, the use of a frequency $\omega$ cannot be justified by a Fourier but by a Laplace transform; its inversion is obtained by an integral on a path in the complex-$\omega$ plane, which must lie above (*i.e.* at larger imaginary part than) any singularity. In Eq. (18) the singularity is at $s$ such that $\omega = m\Omega(s)$, and we must compute the integral in the right-hand side as if $\omega$ had a positive real part. One finds easily that this means that the pole $s_{cor}$ lies below the real-$s$ axis, so that the integration can be done on the contour shown in Fig. 1: away from the pole the path stays on the real-$s$ axis, so that its contribution is the principal part of the integral: this is essentially real, so that it only contributes to a small change of the real part of $\omega$.

The rest of the integration contour is a half-circle around the pole, described clockwise because the pole (when the inverse Laplace transform is properly defined, *i.e.* when $\omega$ has a positive imaginary part) is below the real axis: its contribution to the integral is thus, from Cauchy's theorem, $-i\pi$ times the residue of the integrand at the pole. This gives:

$$\delta\omega \int_{s_{min}}^{s_{max}} ds\; 2\frac{B_0^2}{\Sigma}\left|\frac{\partial}{\partial s}\Phi_M\right|^2 \frac{\partial}{\partial\omega}\left(\frac{1}{L}\right) = \frac{i\pi}{\partial\tilde{\omega}/\partial s}\left[8m\frac{\Omega^2 W}{L^2}\frac{B_0^2}{\Sigma}\left|\Phi_M\right|^2 \quad \frac{\partial}{\partial s}\ln\left(\frac{W\Sigma}{B_0^2}\right)\right]_{corot}$$

or:

$$\delta\omega \int_{s_{min}}^{s_{max}} ds\; 2\frac{B_0^2}{\Sigma}\left|\frac{\partial}{\partial s}\Phi_M\right|^2 \left(\frac{-2\tilde{\omega}}{L^2}\right) = -8i\pi\left[\frac{\Omega^2 W}{\Omega' L^2}\frac{B_0^2}{\Sigma}\left|\Phi_M\right|^2 \frac{\partial}{\partial s}\ln \quad \left(\frac{W\Sigma}{B_0^2}\right)\right]_{corot} \qquad (19)$$

where the square bracket in the right-hand side is evaluated at the pole. The main contribution to the integral on the left-hand side comes form the inner cavity, at $\tilde{\omega} < 0$. This integral is thus real and positive. On the right-hand side, $\Omega'$ is usually negative, so that we get the sign of the growth rate $\gamma = \mathrm{Im}(\omega)$ resulting from the resonance:

$$\mathrm{sign}(\gamma) = \mathrm{sign}\left[\frac{\partial}{\partial s}\ln\left(\frac{W\Sigma}{B_0^2}\right)\right]_{corot} \qquad (20)$$

Thus outward gradients of $W$ and $\Sigma$ are stabilizing, while an outward gradient of $B_0$ is destabilizing.

The full variational principle given in Appendix A contains a second resonant term, associated with pressure stresses. This term is proportional to the derivative of the specific vorticity (sometimes called *vortensity* in this context):

$$\mathrm{sign}(\gamma)\Big|_{\mathrm{Pressure}} = \mathrm{sign}\left[\frac{\partial}{\partial s}\ln\left(\frac{W}{\Sigma}\right)\right] \qquad (21)$$

There is also a cross term, proportional to $hB$. Thus when magnetic stresses are absent we recover the usual result (Papaloizou & Pringle, 1985; Narayan et al., 1987) on the effect of the corotation resonance. Note that in this case an outward gradient of $\Sigma$ is destabilizing. The result in the general case is a combination of these two contributions.

However another result of the general variational form is that the pressure contribution is proportional to $|\sigma|^2$; on the other hand, and in spite of the parallel mentioned in Sect. (2.3) between $\sigma$ and $B_z^D$, the magnetic contribution is rather proportional to $|\Phi_M|^2$, where $\Phi_M$ is the integral of $B_z^D$. As mentioned in Sect. (3.2), $\sigma$ is evanescent in the forbidden band at corotation, making the effect of the resonance exponentially small in the pressure-driven case. But although $B_z^D$ is also evanescent, $\Phi_M$ is not!

In order to understand this, let us imagine that the perturbed field $B_z^D$ is strictly zero in the forbidden band, so that $\Phi_M$ has its source only in the inner cavity where waves can propagate. Then in the corotation region $\Phi_M$ will have the classical behavior of

an $m$-polar potential in vacuum, varying as $r^{-m}$. This allows it to retain a sizable effect at the corotation radius, and thus to efficiently exchange energy with the Rossby vortex.

It would be of course difficult to find a simple explanation to the stabilizing or destabilizing effect of the corotation resonance, in this case as in the Papaloizou-Pringle instability. The starting point would certainly be that, when the equilibrium field varies across the corotation radius, it results in a variation of the tangential force exerted on the disk by the magnetic potential $\Phi_M$, produced by fluctuations in the inner disk region. This variation (or, in the opposite direction, that due to a gradient in the disk inertia) in turn results in differential azimuthal motions, at the source of the Rossby vortex.

We will not try to get, from the variational principle, an estimate of the resulting growth rate. Rough estimates show that it should be of the order of $v_A/r \sim \beta^{-1/2}\Omega h/r$. We will rather turn now to numerical solution of the equations to confirm our analysis and exhibit explicit solutions.

## 4. Numerical study

### *4.1. The eigenvalue problem*

We solve numerically the set of Eqs. (7 - 10), for the four unknowns $U$, $V$, $h$ and $B_z^D$, by turning it into an eigenvalue problem. To do this we write the equations on a staggered grid, with velocities measured halfway between density grid points.

The magnetic potential appearing in the right-hand side of the equations is expressed through Eq. (3). Special care is needed for the Poisson Kernel, which is divergent at $x = 1$. We use a smoothing, replacing Eq. (5) by:

$$K_m(x) = \frac{x}{\pi}\int_0^\pi \frac{d\vartheta \cos m\vartheta}{(x^2 - 2x\cos\vartheta + 1 + \epsilon^2)^{1/2}} \qquad (22)$$

where $\epsilon$ is of the order of $c_S/r\Omega$, representing the effect of finite disk thickness; we have checked that varying $\epsilon$ does not affect the results presented here. Then, for a grid of $n_G$ points separated by $ds$ we define a vector $\xi$ of length $4n_G$, such that

$$\begin{aligned}
\xi(4i) &= U\left(s = (i+\frac{1}{2})ds\right)\\
\xi(4i+1) &= V\left(s = (i+\frac{1}{2})ds\right)\\
\xi(4i+2) &= h\,(s = i\,ds)\\
\xi(4i+3) &= B_z^D\,(s = i\,ds)
\end{aligned}$$

with $i = 1\ldots n_G$. In this manner our equations can be set as an eigenvalue problem:

$$-i\omega\xi = \mathcal{M}\,\xi \qquad (23)$$

where $\mathcal{M}$ is a ($4n_G$x$4n_G$) matrix. It would be band diagonal if we were dealing with a differential problem, *i.e.* local forces. But the magnetic potential (*i.e.* long range, non-local forces), which turns it into an integro-differential problem, makes $\mathcal{M}$ a full complex matrix, for which we seek eigenvalues and eigenvectors. $\mathcal{M}$ would be hermitian in the absence of the radiating boundary condition at large $s$, and of the corotation resonance.

One usually considers that 1000x1000 is the maximal size of a matrix that can be inverted numerically without excessive accumulation of roundoff errors. This leaves us with a maximum $n_G = 250$: in practice, using the complex integration path described below, we have found this limit largely sufficient to get very good convergence of eigenvalues and eigenvectors, and we have not tried to challenge it. The determination of eigenvalues and eigenvectors is thus done with standard library packages and takes only a few minutes on a modern workstation.

### *4.2. The complex contour in $s$*

The main limit to the precision comes from the vicinity of the corotation radius, where the solution varies rapidly–the more as we consider very weakly amplified solutions, so that the pole lies very close to the real-$s$ axis. We solve this difficulty, and at the same time the outer boundary condition, by solving on an oblique axis in the complex-$s$ plane.

This means that, taking $s_{min} = 0$ without loss of generality (since $s$ is logarithmic), we choose $s_{max}$ complex with a positive imaginary part. This serves at the same time three purposes:

1. It allows us to move the integration axis far from the pole, in order to get a smoother behavior. Given the limited number of grid points we can use, this strongly improves the accuracy of the eigenvalues. On the other hand it allows us to exhibit the eigenvector only on this complex axis, so that its components (the velocities etc.) are not the physical solutions one would obtain by solving on the real axis. However we maintain the obliquity of the integration axis weak enough to limit this problem. In selected cases, where the growth rate is strong enough, we solve on the real-$s$ axis and find, as could be expected, that the solution is significantly modified only at large $s$ (note that our solution on the complex axis *is* correct, but is not the one physically observable in real space).
2. Given the constraints on the inverse Laplace transform, discussed in Sect. 3.1, solution along this oblique axis allows us to correctly describe damped solutions by analytic continuation, as long as the imaginary part of $s_{max}$ is sufficient that the integration contour lies on the correct side. We will see below that this appears in a very obvious manner in the eigenvalue spectra.
3. The boundary condition we apply at $s_{max}$ is the *radiation condition*, also called the *outgoing wave condition*. This condition states simply that we do not want the system to receive information from outside, so that the only perturbation allowed at $s_{max}$ is the wave traveling outward. In our case, far enough beyond corotation that the WKB condition is valid, this translates into accepting only a trailing wave, with a local radial wavenumber $k > 0$. We show in Appendix B.1. that this same obliquity of the integration axis (with Im($s > 0$)) provides a simple and efficient way of implementing this boundary condition.

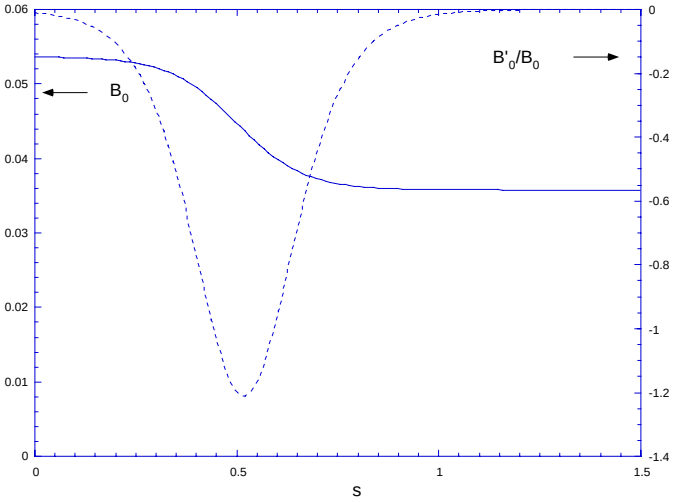


**Fig. 2.** A typical profile of the magnetic field (solid) and its logarithmic derivative (dots). We have a strong but localized gradient, resulting in a limited total change of $B_0$. A similar profile is used for the surface density of the disk

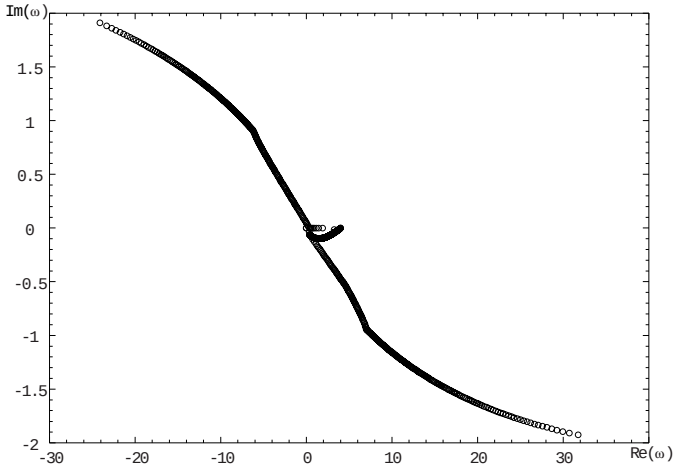


**Fig. 3.** The full spectrum of eigenvalues in a typical low-field case, with $\beta = 50.$ and $m = 4$. Integration is performed on an oblique complex axis $s = (0.,\ 0.)$ to $(1.5,\ 0.1)$. Most of the eigenvalues are associated to the discretization of the system.

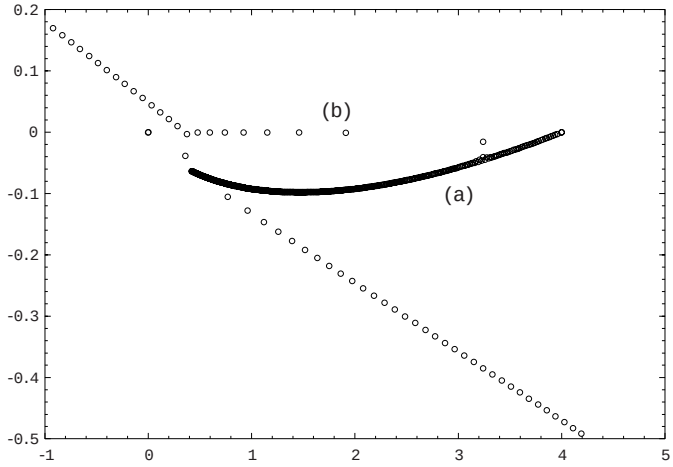


**Fig. 4.** A zoom on the results of Fig. 3. Most noticeable are (a) a dense component corresponding to a continuous spectrum with corotation on the integration axis (b) another component corresponding to the physical discrete spectrum, close to Im($\omega$)=0.

### *4.3. The profiles*

We wish to describe an equilibrium with gradients of density and vertical magnetic fields. On the other hand we do not wish too strong changes of these quantities, which would cause large differences in the radial wavelengths and thus create numerical problems. Thus we use the analytical result, showing that amplification depends only on the local gradients at corotation. This allows us to take profiles with strong but localized gradients, giving limited total variations across the integration domain:

$$\begin{aligned} \Sigma(s) &= \Sigma_0 \left[1. - d_\Sigma \tanh\left(p_\Sigma(s - s_0)\right)\right] \\ B_0(s) &= B_{0int} \left[1. - d_B \tanh\left(p_B(s - s_0)\right)\right] \end{aligned} \quad (24)$$

Using $d_\Sigma$ or $d_B \sim 0.2$ gives reasonable profiles for our purpose. This does not claim to represent realistic profiles, but allows us an optimal study of the physics involved. Fig. 2 shows a typical profile of the magnetic field and its logarithmic derivative. When needed we use trial and errors, on low-precision runs with a limited number of points, to change $s_0$ so that the corotation radius lies close to the maximal gradient.

### *4.4. Numerical results*

We measure the strength of the magnetic field by the usual parameter giving the ratio of thermal to magnetic pressure:

$$\beta = \frac{8\pi p}{B_0^2}$$

taken at the inner disk radius. At low field ($\beta \gg 1$) we expect the magnetic component of the perturbation to play only a weak role. Furthermore, this is the regime where the magneto-rotational instability is unstable and should dominate anomalous viscosity. Nevertheless we will present numerical results at $\beta = 50$, in order to check the general physics presented here. In contrast we will show a second set of results for $\beta = 1$, where our instability is obtained while the magneto-rotational instability (which does not appear in our analysis since we consider infinitely thin disks) should be stable.

We use the result of Eq. (19) to limit the parameters we vary: we keep $\Sigma$ constant and introduce only a radial variation of $B_0$. We use trial and error to have a maximum gradient very near the corotation radius, with

$$\frac{\partial}{\partial s} \ln B_0 \approx 1$$

so that, from Eq. (19), the modes should be weakly unstable if the magnetic contribution dominates, and (from the additional terms included in Eq. (A3)) damped if pressure dominates. We choose a sound speed $c_S = .1 r_0 \Omega_0$, where the subscript 0 notes values at the inner radius ($s = 0$). Figs. 3–4 show the spectrum of eigenvalues we obtain for $\beta = 50$ and $m = 4$. Frequencies

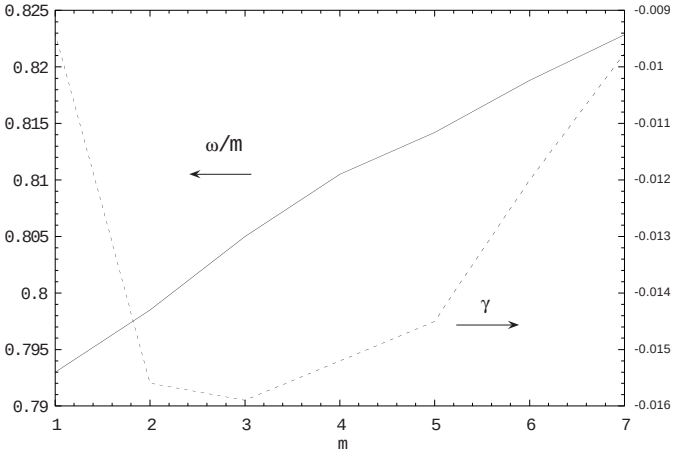


**Fig. 5.** Real (full line) and imaginary (dashed) parts of the $n = 0$ eigenvalue for $\beta = 50$. All the modes are damped by the corotation resonance.

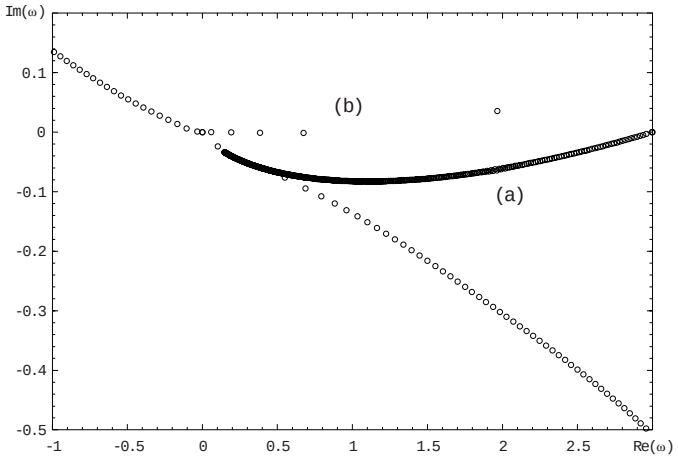


**Fig. 6.** The spectrum for $\beta = 1$, $m = 3$. The fundamental mode has a significant positive real part, *i.e.* is amplified by the corotation resonance.

are normalized with $\Omega_0 = 1.$, so that eigenvalues whose real part lie between 0 and $m$ have a corotation at $s > 0$.

We distinguish three components in the spectrum:

1. a set of values aligned diagonally, as seen in Fig. 3. From their behavior as the number $n_s$ of grid points is varied, we find these values to form a continuous spectrum as $n_s \to \infty$, associated with the discretization of the problem, and thus not physical.
2. A second component, labeled (a) in Fig. 4. These also form a continuous spectrum, and correspond to unphysical solutions with corotation very near grid points: thus when we solve along a real-$s$ axis, this component lies on the real-$\omega$ axis. This permits us to directly check on the plots that all roots above this set, even when (as here) they are weakly damped, lie on the proper side of the integration axis, as discussed in Sect. 4.2.
3. A third component, labeled (b) in Fig. 4, corresponds to a discrete spectrum. In order of decreasing $\omega$, these eigenvalues correspond to the classical set of modes with $n = 0,\ 1,\ 2, \ldots$ nodes in their radial structure, between the inner radius and corotation. Due to the limited numerical precision, the frequency of only the fundamental solution, $n = 0$, is reliable, although higher-order ones do show the increasing number of nodes, verifying our identification of this discrete spectrum. The $n = 0$ eigenvalue converges to a very good accuracy when $n_s$ is varied above typically 200.

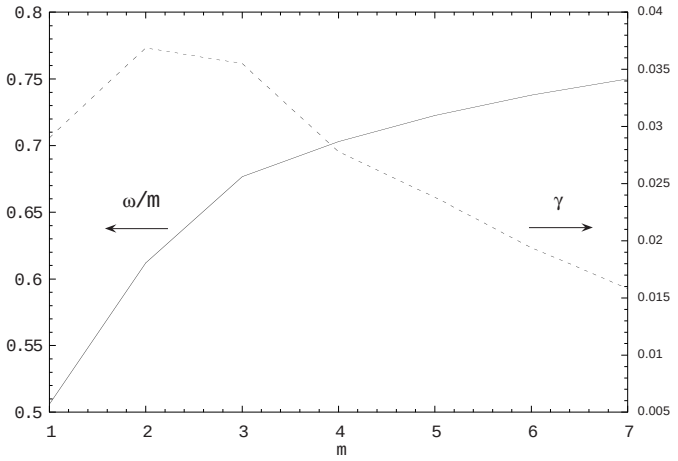


**Fig. 7.** Real (full line) and imaginary (dashed) parts of the $n = 0$ eigenvalue for $\beta = 1$. The modes have become unstable by the corotation resonance.

Fig. 5 shows the variations of the pattern frequency, $\omega/m$, and growth rate, $\gamma = \mathrm{Im}(\omega)$, as a function of $m$. At this high value of $\beta$, the modes are all weakly damped by the corotation resonance, according to Eq. (21).

On the other hand, Fig. 6 shows the spectrum for $\beta = 1.$, $m = 3$. The fundamental mode has acquired a significant positive imaginary part, *i.e.* becomes unstable by the corotation resonance. Fig. 7 shows that low-$m$ modes become unstable. The growth rate is not strong (e.g. for $m = 2$, $\gamma$ is 0.06 times the pattern frequency), but one has to remember that we are dealing with normal modes, *i.e.* long-lived, exponentially amplified structures, so that this may result in strong amplitudes after a finite time.

We show on Fig. 8 the mode frequency and growth rate for $m = 2$, as a function of $\beta$. The frequency decreases as $\beta$ decreases, while the growth rate has a maximum for $\beta$ close to 1. This can be understood from the dispersion relation, Eq. (17): at low $\beta$ the wavelength becomes larger, widening the "cavity" and thus pushing to larger $r$ the corotation radius; on the other hand the turning point (the radius where the radial wavenumber $k_s = 0$) is in fact not exactly at the Lindblad resonance, but where

$$\tilde{\omega}^2 - \kappa^2 = \frac{2B_0^2}{\Sigma}\frac{m}{r} + \frac{m^2}{r^2}c_S^2 \tag{25}$$

so that the forbidden band around corotation widens as $\beta$ decreases. Thus at low $\beta$ the amplification mechanism becomes less efficient.

Finally we show on Figs. 9–10 the eigenvector for a typical mode, showing in particular the cavity inside corotation and

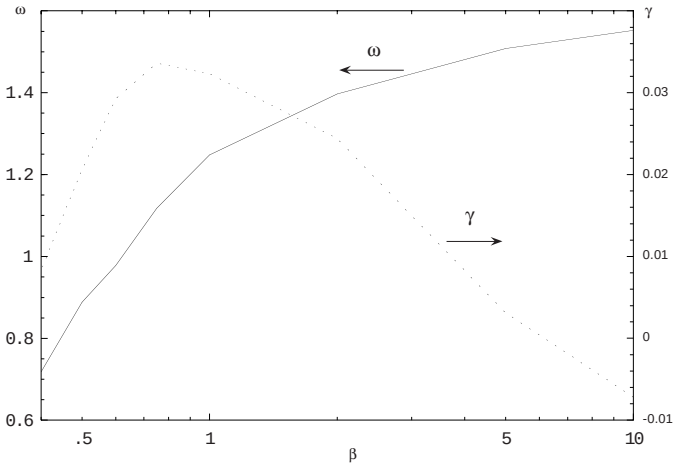


**Fig. 8.** The frequency and growth rate as a function of $\beta$, for the $m = 2$ mode.

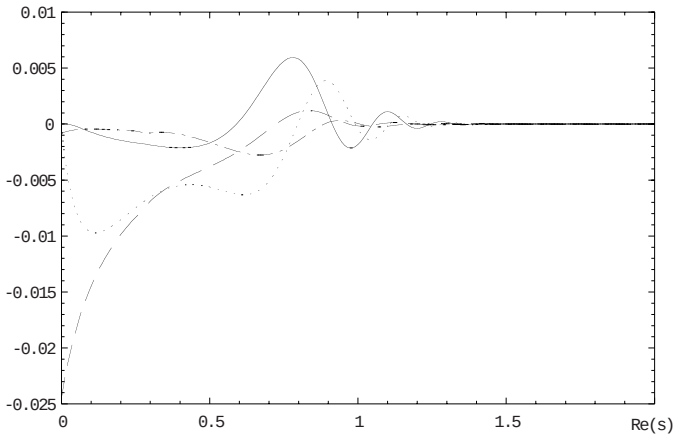


**Fig. 9.** The eigenvector: Real (solid) and imaginary (dots) parts of U, Real (dashes) and imaginary (dash-dots) parts of V for $\beta = 1$, $m = 3$. Corotation is at $s = .28$.

outgoing wave beyond it, decreasing at large $s$ because of the obliquity of the integration axis.

## 5. Discussion

We have presented an instability of magnetized accretion disks, which has the important potential of relating accretion (by a spiral density wave in the disk) and ejection, through Alfven waves propagating to the corona of the disk the energy and angular momentum extracted by the spiral. The instability has the following characteristics:

- It forms *normal modes*, *i.e.* standing, exponentially growing, wave patterns.
- Their growth rate is rather small, typically of the order of $h\Omega/r$ where $h$ is the disk thickness (we could have shown stronger growth rates by increasing the gradients in our numerical examples). But their exponential behavior still allows them to reach high amplitudes in a finite time.
- The modes are localized in the innermost part of the disk: since the sound and Alfven velocities are small compared to the rotation velocity, the wavelength in the "cavity", between the inner radius and the ILR, is of the order of a few times the disk thickness (we will not discuss here the exact relationship, which is not important). Thus the frequency of the fundamental mode (with no node in the cavity) is essentially fixed, at a given $m$, by the existence of an ILR close to the inner disk radius: $\omega - m\Omega = -\kappa$ at $r = r_i$ close to the inner radius $r_0$, with $\Omega = \kappa$ in a keplerian disk, gives $\omega = m\Omega(r_c) = (m-1)\Omega(r_i)$, where $r_c$ is the corotation radius, and thus

$$r_c = \left(\frac{m}{m-1}\right)^{2/3} r_i$$

  Thus these modes cannot be considered as candidates to explain accretion in the bulk of the disk, but only to energize jets close to the inner radius, where, in usual viscous models, half of the energy and momentum of accretion are deposited in a boundary layer. Actually the size of the "cavity" is such that it might be considered as a form of boundary layer.
- The instability occurs in strongly magnetized disks, with $\beta \lesssim 1$ (where the magneto-rotational instability is stable)
- It appears when the quantity $\Omega\Sigma/B_0^2$ increases radially. This requires either an inverted density gradient, or a strong magnetic field gradient. This means that disk models must consider the radial transport of magnetic flux, as well as that of the accreted matter: the horizontal part of the magnetic flux can be expelled from the disk vertically by buoyancy (e.g. the Parker instability, Foglizzo & Tagger, 1994, 1995), but the vertical part can only accumulate in the central region of the disk, if the accretion turbulence transports it together with the matter. One may note as an example that at the center of our galaxy, on a scale of $\sim 100\,$pc, the magnetic field seems to be vertical and of the order of a few milligauss, as compared with a horizontal field of a few $\mu$gauss elsewhere in the galactic disk.

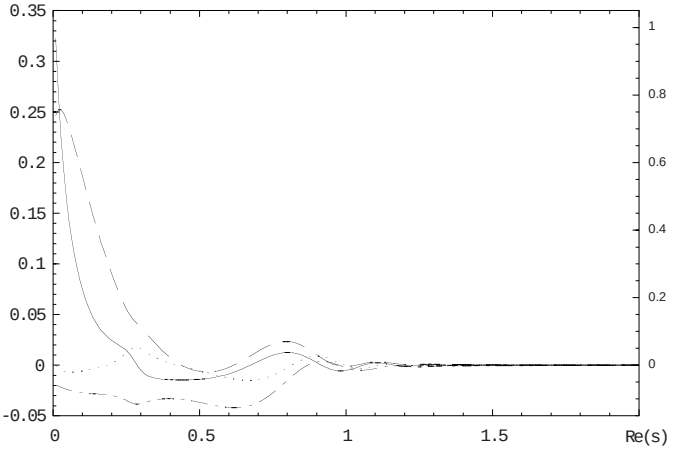


**Fig. 10.** The eigenvector: Real (solid) and imaginary (dots) parts of $\sigma$, Real (dashes) and imaginary (dash-dots) parts of $\Phi_M$ for $\beta = 1$, $m = 3$. Corotation is at $s = .28$.

This threshold in radial gradients also implies that this instability is very likely to result in a bursty behavior of the ac-

cretion/ejection process, associated with the processing of both gas *and magnetic flux* in the disk.

We also wish to mention the possible connection between this instability and the QPOs observed in X-ray binaries: since the mechanism favors low $m$ values, *i.e.* spirals with a small number of arms, it is very likely to appear as very coherent, monochromatic structures, in the manner of galactic spirals. Their corotation radius would be of the order of a few times the inner disk radius. These are precisely characteristics of the low frequency QPOs, with a frequency in the range of 0.1 (in black hole binaries) to a few tens (in neutron star binaries) of Hertz (see e.g. Wijnands & Van der Klis, 1999), *i.e.* a frequency typical of keplerian rotation not far from the inner disk boundary (Markwardt et al., 1999; Psaltis et al., 1999).

*Acknowledgements.* The authors gratefully acknowledge many helpful discussions with T. Foglizzo, J. Goodman, R.N. Henriksen and J. Papaloizou. Part of this work was completed at the Isaac Newton Institute for Mathematical Sciences (Cambridge) while one of us (MT) attended the program on Astrophysical Disks.

## Appendix A: the full variational principle

In this appendix we perform essentially the same computations as in Sect. (3.1), but retaining pressure stresses to give a complete variational principle.

Thus Eq. (15) becomes:

$$
\begin{aligned}
r^2 B_z^D = &-\frac{\partial}{\partial s}\left(\frac{2}{L}\frac{B_0^2}{\Sigma}\frac{\partial}{\partial s}\Phi_M\right) - \frac{\partial}{\partial s}\left(\frac{B_0}{L}\frac{\partial}{\partial s}c_S^2 h\right)\\
&+\frac{2B_0^2}{\Sigma L^2}\Phi_M\Bigg\{m^2\left(L+4\Omega\Omega'\right)\\
&+2m\Omega\left[\tilde{\omega}\frac{\partial}{\partial s}\ln\left(\frac{\Omega B_0^2}{\Sigma}\right)+2\frac{\Omega W}{\tilde{\omega}}\frac{\partial}{\partial s}\ln\left(\frac{W\Sigma}{B_0^2}\right)\right]\Bigg\}\\
&+\frac{B_0}{L^2}c_S^2 h\Bigg\{m^2\left(L+4\Omega\Omega'\right)\\
&+2m\Omega\left[\tilde{\omega}\frac{\partial}{\partial s}\ln\left(\Omega B_0\right)+2\frac{\Omega W}{\tilde{\omega}}\frac{\partial}{\partial s}\ln\left(\frac{W}{B_0}\right)\right]\Bigg\} \qquad \text{(A1)}
\end{aligned}
$$

In the same manner, starting from Eq. (9) we obtain a similar equation for $\sigma$:

$$
\begin{aligned}
r^2\sigma = &-\frac{\partial}{\partial s}\left(\frac{2B_0}{L}\frac{\partial}{\partial s}\Phi_M\right) - \frac{\partial}{\partial s}\left(\frac{\Sigma}{L}\frac{\partial}{\partial s}c_S^2 h\right)\\
&+\frac{2B_0}{L^2}\Phi_M\Bigg\{m^2\left(L+4\Omega\Omega'\right)\\
&+2m\Omega\left[\tilde{\omega}\frac{\partial}{\partial s}\ln\left(\Omega B_0\right)+2\frac{\Omega W}{\tilde{\omega}}\frac{\partial}{\partial s}\ln\left(\frac{W}{B_0}\right)\right]\Bigg\}\\
&+\frac{\Sigma}{L^2}c_S^2 h\Bigg\{m^2\left(L+4\Omega\Omega'\right)\\
&+2m\Omega\left[\tilde{\omega}\frac{\partial}{\partial s}\ln\left(\Omega\Sigma\right)+2\frac{\Omega W}{\tilde{\omega}}\frac{\partial}{\partial s}\ln\left(\frac{W}{\Sigma}\right)\right]\Bigg\} \qquad \text{(A2)}
\end{aligned}
$$

We multiply Eq. (A2) by $c_S^2 h^*$, and Eq. (A1) by $2\Phi_M^*$, sum the results and integrate over $s$: this gives, after integrations by parts, the full variational principle similar to Eq. (15):

$$
\begin{aligned}
&\int_{s_{min}}^{s_{max}} ds\Bigg\{r^2(s)\left[c_S^2 h^*\sigma + 2\Phi_M^*(s)B_z^D(s)\right]\\
&-\frac{2B_0 c_S^2}{L}\left[\left(\frac{\partial}{\partial s}h^*\right)\left(\frac{\partial}{\partial s}\Phi_M\right)+\left(\frac{\partial}{\partial s}\Phi_M^*\right)\left(\frac{\partial}{\partial s}h\right)\right]\\
&-\frac{1}{L}\left[\Sigma c_S^4\left|\frac{\partial}{\partial s}h\right|^2 + 4\frac{B_0^2}{\Sigma}\left|\frac{\partial}{\partial s}\Phi_M\right|^2\right]\\
&-\frac{2B_0}{L^2}c_S^2\left[h^*\Phi_M + h\Phi_M^*\right]\Bigg\{m^2\left(L+4\Omega\Omega'\right)\\
&\quad+2m\Omega\left[\tilde{\omega}\frac{\partial}{\partial s}\ln\left(\Omega B_0\right)+2\frac{\Omega W}{\tilde{\omega}}\frac{\partial}{\partial s}\ln\left(\frac{W}{B_0}\right)\right]\Bigg\}\\
&+\frac{\Sigma}{L^2}c_S^4|h|^2\Bigg\{m^2\left(L+4\Omega\Omega'\right)\\
&\quad+2m\Omega\left[\tilde{\omega}\frac{\partial}{\partial s}\ln\left(\Omega\Sigma\right)+2\frac{\Omega W}{\tilde{\omega}}\frac{\partial}{\partial s}\ln\left(\frac{W}{\Sigma}\right)\right]\Bigg\}\\
&+\frac{4B_0^2}{\Sigma L^2}|\Phi_M|^2\Bigg\{m^2\left(L+4\Omega\Omega'\right)\\
&+2m\Omega\left[\tilde{\omega}\frac{\partial}{\partial s}\ln\left(\frac{\Omega B_0^2}{\Sigma}\right)+2\frac{\Omega W}{\tilde{\omega}}\frac{\partial}{\partial s}\ln\left(\frac{W\Sigma}{B_0^2}\right)\right]\Bigg\}\Bigg\}\\
&=-\Bigg[\frac{2B_0}{L}c_S^2\left(h^*\frac{\partial}{\partial s}\Phi_M+\Phi_M^*\frac{\partial}{\partial s}h\right)\\
&\quad+\frac{\Sigma}{L}c_S^4 h^*\frac{\partial}{\partial s}h + \frac{4B_0^2}{\Sigma L}\Phi_M^*\frac{\partial}{\partial s}\Phi_M\Bigg]_{s_{min}}^{s_{max}} \qquad \text{(A3)}
\end{aligned}
$$

As in Eq. (15) the left-hand side is hermitian, so that this is again a variational principle.

## Appendix B: boundary conditions

### *B.1. Outer boundary: outgoing wave*

As explained in Sect. 4.2, we require that at the outer boundary the solution reduces to an outgoing wave. The complex integration axis allows us an easy implementation of this condition. We start by assuming that $s_{max}$ is large enough that the WKB approximation can be used.

Then let us consider the two WKB solutions:

$$\xi_\pm \sim \exp\left(\pm i\int^s ds' k(s')\right)$$

where the plus and minus sign correspond respectively to the trailing (outgoing) and leading (incoming) waves. If we integrate on an oblique axis in the complex-$s$ plane, with Im($s$) positive, one sees that the trailing solution decreases exponentially, while the leading one grows exponentially, as $s$ increases.

Let us now assume that we have at $s_{max}$ an incorrect boundary condition. In general, this means that we have leading and trailing waves of

comparable amplitude. But as one goes inward from $s_{max}$, the trailing solution grows exponentially as $s$ decreases while the leading one decreases. Thus at some distance inward from $s_{max}$ the correct (trailing) solution will dominate. This method of dealing with the boundary condition has been introduced in disk physics by Drury (1980). It allows us here to take any simple (but a priori false) boundary condition at $s_{max}$, and only check a posteriori that the correct behavior results; if it is not the case we just need to increase Im($s_{max}$). In practice we use a reflecting condition at $s_{max}$ and have little difficulty with the outer boundary condition.

In fact we have another effect helping us with the outer boundary condition: as seen from the WKB dispersion relation, Eq. (17), the wavelength becomes small at large $s$. On the other hand our numerical scheme for the discretization of the equations is such that, when the wavelength becomes comparable with the grid spacing, waves suffer a heavy numerical damping. Then if we have a solution resulting in an outgoing wave, this wave is damped at large $s$ and very little of its energy can be reflected. Thus taking Re($s_{max}$) large enough is also a good way of implementing the outer boundary condition.

Let us now turn to the contribution of the outer boundary to the variational principle, Eq. (15). It is easily obtained in the WKB approximation,

$$\frac{\partial}{\partial s}\Phi_M = ik\Phi_M$$

with $k$ given by the dispersion relation, Eq. (17). Let us treat this boundary term by perturbations, as we do for the resonance term: we see that, since it is imaginary, its contribution will be to the growth rate of the mode. In fact one easily checks that with $k > 0$ (for an outgoing wave) it is always destabilizing, as mentioned in Sect. (3.2). This is the amplification mechanism discussed, in the shearing sheet approximation, in paper I. The resulting growth rate is always quite small.

### *B.2. Inner boundary: reflection*

Any condition at the inner edge of the disk, which does not change the energy of the wave, will reflect it with an efficiency of 1. This is the classical picture leading to normal modes. Various conditions satisfy this criterion, and we discuss them here with the help of the variational principle. For simplicity we will discuss here only the pressureless variational principle of Eq. (15), but the generalization to the complete problem is straightforward.

From Eq. (15) we see that by making either

$$\Phi_M = 0 \tag{B1}$$

or

$$\frac{\partial}{\partial s}\Phi_M = 0 \tag{B2}$$

the boundary term vanishes, so that the mode energy is not changed. Either of these conditions is thus an acceptable reflecting boundary condition.

On the other hand it is more usual to assume a rigid boundary and require that

$$U = 0 \tag{B3}$$

at the inner edge. In this case Eqs. (7-8), forgetting the pressure terms, give:

$$4im\frac{B_0^2}{\Sigma^2}\Phi_m^*\frac{\partial}{\partial s}\Phi_M = 2i\tilde{\omega}^*\Omega\left|V\right|^2 \tag{B4}$$

making the boundary term real. Thus if we start from a marginal mode ($\omega$ real) with boundary conditions (B1) or (B2), and change it to $U = 0$, the resulting change to $\omega$ is real: this means that condition (B3) also gives a perfect reflection of the wave, but with a different phase; the resulting change in the integral phase condition modifies the discrete set of mode frequencies, but does not introduce growth or damping. We note that the condition $V = 0$ used by NGG would give a similar result. We use condition (B3) in the numerical solutions.

## Appendix C: emission of Alfven waves in the WKB limit

In this appendix we describe in the simplest manner the emission of Alfven waves, carrying some of the energy and angular momentum of the density waves in the disk to its corona if the latter has a small but non-vanishing density (thus relaxing the hypothesis, made throughout the paper, that the disk lies in vacuum). We do this in a simple WKB limit in the region where density waves propagate radially, ie far from the corotation region. A full computation, without the WKB approximation, would be necessary to describe the emission of energy and momentum from the vortex at corotation. We defer it to a future publication.

In order to describe the vertical propagation of the Alfven waves, we now consider the $z$ dendence of the variables. We start from the Euler equations and derive equations for two new quantities:

$$\begin{aligned} D(s,z) &= \frac{\partial}{\partial s}U + imV = r^2\boldsymbol{\nabla}_\perp\cdot\boldsymbol{V}_\perp \\ R(s,z) &= \frac{\partial}{\partial s}V - imU = r^2\boldsymbol{\nabla}_\perp\times\boldsymbol{V}_\perp \end{aligned}$$

where the subscript $\perp$ refers to the components of a vector in the plane of the disk. We get:

$$-i\tilde{\omega}D - 2\Omega R - 2\Omega'(v - imu) = r^2\boldsymbol{\nabla}\cdot(\boldsymbol{F}/\rho_0) \tag{C1}$$

$$-i\tilde{\omega}R + WD + W'u = r^2\boldsymbol{\nabla}\times(\boldsymbol{F}/\rho_0) \tag{C2}$$

where $\rho_0(s,z)$ is the equilibrium density, and $\boldsymbol{F}$ is the perturbed force acting on the fluid. Here for simplicity we will again neglect pressure forces, unimportant for Alfven waves.

We now use the WKB approximation, by defining a local radial wavenumber

$$\frac{\partial}{\partial s} \simeq ik$$

with $k \gg m$. The dispersion relation, Eq. (17), tells us that this is verified far from corotation. Consistently neglecting all radial gradients of equilibrium quantities, and using the induction equation for the perturbed magnetic field, we get after some algebra:

$$-i\tilde{\omega}D - 2\Omega R = \frac{v_A^2}{i\tilde{\omega}}\left(\frac{q^2}{r^2} - \frac{\partial^2}{\partial z^2}\right)D \tag{C3}$$

$$-i\tilde{\omega}R + WD = -\frac{v_A^2}{i\tilde{\omega}}\frac{\partial^2}{\partial z^2}R \tag{C4}$$

We now use the same procedure as in Tagger et al. (1992): let us assume that at large $z$ ($z \gg h$, where $h$ is the disk scale height) the density goes to a small but non-vanishing density $\rho_\infty$ mimicking a disk corona. There $v_A$ becomes very large, so that Eq. (C3) gives to lowest order:

$$D(z) \sim e^{-|kz|}$$

where the minus sign comes from the condition that $D$ decreases at infinity. Thus we get the same behavior derived for $\Phi_M$ in the case where the disk lies in vacuum. On the other hand Eq. (C4) gives:

$$R(z) \sim e^{ik_z z}$$

where

$$k_z = \frac{\tilde{\omega}}{v_A^\infty},\ v_A^{\infty 2} = \frac{B_0^2}{4\pi\rho_\infty}$$

and causality requires that $k_z$ has the same sign as $\tilde{\omega}$, so that this describes an Alfven wave emitted from the disk.

We now multiply Eqs. (C3-C4) by $\rho(z)$ and integrate over $z$. We get:

$$-i\tilde{\omega}\bar{D} - 2\Omega\bar{R} = \frac{\overline{v_A^2}}{i\tilde{\omega}}\frac{q}{rh}\bar{D} \quad \text{(C5)}$$

$$-i\tilde{\omega}\bar{R} + W\bar{D} = -\frac{\overline{v_A^2}}{i\tilde{\omega}h}ik_z\bar{R} \quad \text{(C6)}$$

where the bar means an average over the disk height, and the right-hand side of Eq. (C5) is an estimate of the integral, which allows us to recover in the limit $\rho_\infty \to 0$ the dispersion relation, Eq. (17). From these equations we get the dispersion relation when the coronal density is small:

$$\tilde{\omega}^2 = \kappa^2 + \frac{|k|}{rh}\overline{v_A^2} - i\frac{k_z}{\tilde{\omega}^2 h}\kappa^2\overline{v_A^2} \quad \text{(C7)}$$

Using the value of $k_z$, and solving by perturbation, we find that the emission of Alfven waves to the corona results in a damping of the density wave, *i.e.* $\omega$ gets a negative imaginary part:

$$\gamma_{Alfven} \simeq -\frac{1}{2\tilde{\omega}^2\beta^{1/2}}\kappa^2\Omega\left(\frac{\rho_\infty}{\rho_0}\right)^{1/2} \quad \text{(C8)}$$

where $\rho_0$ is the density at the midplane of the disk. From this result we can get the following conclusions:

- The damping is proportional to the square root of the density at infinity, a result typical of magnetic breaking.
- It applies through $R$, the torsional component of the perturbation: as expected, $R$ involves a torsional (in contrast with $D$, giving a compressional) motion of the footpoints of the field lines in the disk. This motion propagates to the corona as an Alfven wave. It is noteworthy that $R$ is singular at corotation, because of the vorticity gradient contribution ($W'u$) in Eq. (C2), and indeed represents the Rossby vortex there - although this is not described in the WKB approximation used in this appendix. Thus we can expect a strong Alfven wave emitted from thee Rossby vortex at corotation.
- This may be even stronger, since Eq. (C8) shows a vanishing denominator at corotation. This must of course be taken only as an indication, since the WKB approximation vanishes in this region.

The full computation of this effect would need to relax the WKB approximation. Its consequences on the formation of a jet requires nonlinear study of the deposition of Alfven wave energy in the corona. These extensions of our result will be the object of future work.

## References


Balbus, S.A., Hawley, J.F., 1991, ApJ 376, 214
Binney, J., Tremaine, S., 1987, *Galactic Dynamics*, Princeton University Press
Blandford, R. D., Payne, D. R. 1982, MNRAS 199, 883
Cabrit, S., André, P., 1991, ApJ 379, L25
Chandrasekhar, S., 1960, Proc. Nat. Acad. Sci. 46, 253
Curry, C., Pudritz, R., 1996, MNRAS 281, 119
Drury, L. O'C., 1980, MNRAS 193, 337
Edwards, S., Ray, T. P., Mundt R., 1993, *in Protostars and Planets III*, ed. E. Levy, J. Lunine (Tucson: Univ. of Arizona Press), 567
Ferreira, J., Pelletier, G., 1993, A&A 276, 625
Foglizzo, T., Tagger, M., 1994, A&A 287, 297
Foglizzo, T., Tagger, M., 1995, A&A 301, 293
Lin, C.C., 1955, *The theory of Hydrodynamic Stability*, Cambridge University Press, London
Markwardt, C.B., Swank, J., Taam, R.E., 1999 to appear in ApJ *Letters*
Mirabel, I. F., Dhawan, V. Chaty, S., Rodriguez, L. F., Marti, J., Robinson, C. R.; Swank, J., Geballe, T., 1998, A&A 330, L9
Morse, P.M., Feshbach, H., 1953, *Methods of Theoretical Physics*, McGraw Hill book company, Inc., New York
Narayan, R., Goldreich, P., Goodman, J., 1987, MNRAS 228, 1
Ogilvie, G.I., Livio, M., 1998, ApJ 499, 329
Pannatoni, R.F., 1983, Geophys. Ap. Fluid Dyn. 24, 165
Papaloizou, J.C.B., Pringle, J.E., 1984, MNRAS 208, 721
Papaloizou, J.C.B., Pringle, J.E., 1985, MNRAS 213, 799
Pelletier, G., Pudritz, R. E. 1992, ApJ 394, 117
Psaltis, D., Belloni, T., Van der Klis, M., 1999, to appear in ApJ
Shakura, N.I., Sunyaev, R.A., 1973 A&A, 24, 337
Spruit, H.C, Taam, R.E., 1990, A&A 229, 475
Spruit, H.C., Stehle, R., Papaloizou, J.C.B., 1995, MNRAS 275, 1223
Stehle, R., Spruit, H.C., 1998, *submitted to* MNRAS
Tagger, M., Henriksen, R.N., Sygnet, J.F., Pellat, R., 1990, ApJ 353, 654 (Paper I)
Tagger, M., Pellat, R., Coroniti, F., 1992, ApJ 393, 708
Velikhov, E.P., 1959 Sov. Phys. JETP Lett. 9, 995
Wijnands, R., Van der Klis, M., 1999, ApJ 514, 939